

First-order magneto-structural transition in single crystals of the honeycomb lattice Ruthenate Li_2RuO_3

Kavita Mehlaawat and Yogesh Singh

*Indian Institute of Science Education and Research (IISER) Mohali,
Knowledge city, Sector 81, Mohali 140306, India*

(Dated: May 31, 2016)

Li_2RuO_3 is known to crystallize in either $C2/m$ or $P2_1/m$ structures at room temperature. We report the first single crystal growth of Li_2RuO_3 and Na substituted crystals $(\text{Li}_{0.95}\text{Na}_{0.05})_2\text{RuO}_3$ crystallizing in the $P2_1/m$ structure where a magneto-structural transition is observed at high temperatures. Using high temperature ($T \leq 1000$ K) magnetic susceptibility χ measurements we study the magnetic anisotropy across the magneto-structural transition. Our results show for the first time that for Li_2RuO_3 the magnetic and structural transitions most likely occur at slightly different temperatures. The structural transition which is first order-like occurs first ($T \approx 570$ K) and drives the magnetic transition ($T \approx 540$ K). Rather surprisingly, just 5% Na substitution for Li affects the magneto-structural transition in an interesting way. The first order transition temperature stays ≈ 540 K, the magnetic anisotropy is reversed, and the Ru-Ru dimerization pattern changes from two short and four long Ru-Ru bonds per honeycomb in an armchair pattern for Li_2RuO_3 to four short and two long bonds per honeycomb in $(\text{Li}_{0.95}\text{Na}_{0.05})_2\text{RuO}_3$ which can be viewed as two inter-penetrating armchair patterns.

I. INTRODUCTION

Mott insulators with spin-orbit (SO) coupling have recently been topics of great interest because of the plethora of novel phases and behaviors they are expected to exhibit¹⁻³. Iridium based transition metal oxides are ideal systems to investigate the novel behaviors predicted to arise due to the interplay of electron correlations and SO coupling^{3,4}. In recent years honeycomb lattice iridates A_2IrO_3 ($\text{A} = \text{Na}, \text{Li}$) have been subjects of intense scrutiny which was fuelled initially by the suggestion of exotic topological properties and Quantum Spin Hall effect^{2,5} and by suggestions that these could be realizations of the Kitaev-Heisenberg model^{1,6}. Na_2IrO_3 was found to undergo novel magnetic ordering at low temperatures suggesting that it wasn't situated in the strong Kitaev limit where a spin liquid was expected^{7,8}. Recently however, evidence for dominant bond-directional magnetic exchange and real space-magnetic moment locking has been found in Na_2IrO_3 ⁹. For ruthenates, the spin-orbit coupling is expected to be comparatively smaller. Nevertheless the compound $\alpha\text{-RuCl}_3$, which has a network of Ru^{3+} $S = 1/2$ moments on a honeycomb lattice has recently been studied in the quest for a candidate Kitaev material¹⁰. Observations of a quasi-continuum of excitations in Raman scattering for both Na_2IrO_3 and $\alpha\text{-RuCl}_3$ has been argued to be evidence for proximity to the quantum spin liquid state in the dominant Kitaev limit^{11,12}. More recently, when Ir^{4+} was partially replaced by Ru^{4+} in $\text{A}_2\text{Ir}_{1-x}\text{Ru}_x\text{O}_3$ ($\text{A} = \text{Na}, \text{Li}$), the materials were found to remain insulating and a spin-glass state is observed at low temperatures highlighting the presence of competing interactions and phases in the parent iridate compounds^{13,14}.

The ruthenate family A_2RuO_3 ($\text{A} = \text{Na}, \text{Li}$) is also known to adopt a honeycomb lattice structure but with nominal $S = 1$ moments arising from the low-spin state

of Ru^{4+} . Polycrystalline samples of Na_2RuO_3 were reported to crystallize in the $C2/c$ structure¹⁵ similar to early reports on Na_2IrO_3 ⁷. More recently, single crystals of Na_2RuO_3 were synthesized and found to crystallize in the related but more symmetric $C2/m$ structure¹⁶. Single crystal Na_2RuO_3 was found to be a local moment magnet which orders antiferromagnetically below $T_N = 30$ K¹⁶.

The structure and magnetic properties of Li_2RuO_3 seem to be very sensitive to synthesis conditions and quality of samples. Initial reports on polycrystalline samples suggested a room temperature $C2/c$ monoclinic structure and metallic paramagnetic behavior below $T = 300$ K¹⁷⁻¹⁹. Later a comprehensive study on polycrystalline samples of Li_2RuO_3 revealed an unusual second order structural phase transition near $T \approx 540$ K from a nearly perfect honeycomb lattice $C2/m$ structure at high temperature to a low temperature structure with a distorted honeycomb lattice $P2_1/m$ ²⁰. This structural transition was accompanied by an increase in resistance and loss of magnetization. Nearly perfect hexagons of the high temperature $C2/m$ phase undergo strong distortion, leading to a low temperature structure with significant shortening of one of the three inequivalent Ru-Ru bonds on each honeycomb²⁰. Based on DFT calculations on the low and high temperature structures it was proposed that Li_2RuO_3 undergoes a transition from a highly correlated metal to a molecular orbital insulator involving Ru-Ru dimerization and spin-singlet formation^{20,21}. An alternative mechanism of spin-singlet formation driven by magnetoelastic coupling has also been proposed²². The evolution of the structural Ru-Ru dimers across the phase transition has been studied recently using pair distribution function (PDF) analysis of high energy powder X-ray data. The PDF analysis allows the tracking of short-ranged structural order. It was found that dynamically fluctuating dimers survive at temperatures well

above the transition temperature $T \approx 540$ K²³. This suggests a scenario where a valence bond crystal in the low temperature phase melts into a valence bond liquid at high temperatures. Such a scenario is supported by recent Ru site dilution experiments²⁴. An electronic structure study has highlighted the importance of electronic correlations and proposed that a combination of local-moment behavior and molecular orbital formation could be the correct picture for this material²⁵.

Recently a careful study of the effect of synthesis conditions on the structure and magnetic behavior of polycrystalline samples has been carried out²⁶. It was found that all samples crystallized in the $P2_1/m$ structure at room temperature and showed the Ru-dimerization transition at high temperatures. However, the details of the structure and the magnetic properties strongly depends on the synthesis conditions. The best quality samples revealed that the magneto-structural transition is first-order in nature with a much higher onset temperature of ≈ 550 K²⁶.

Lastly, single crystals of Li_2RuO_3 have recently been synthesized. The crystals are found to crystallize at room temperature in either the $C2/m$ or the $P2_1/m$ structures depending on synthesis conditions. However, in complete contrast to all existing polycrystalline work^{20,23,24,26}, neither of these crystals show the magneto-structural transitions at high temperature. They instead show Curie-Weiss behavior below 300 K and magnetic ordering at low temperatures into supposedly antiferromagnetic states¹⁶.

In this work we report the first crystal growth of Li_2RuO_3 and 5% Na substituted Li_2RuO_3 crystallizing in the $P2_1/m$ structure at room temperature and showing the magneto-structural transition at high temperatures. We are therefore able to study for the first time the magnetic anisotropy across the high temperature magneto-structural transition. We observe that for Li_2RuO_3 the transition might occur in two steps with a first-order structural transition occurring first (onset ≈ 570 K) which then drives the magnetic Ru-Ru dimerization transition (≈ 540 K). Replacing just 5% Li by Na leads to a reversal of the magnetic anisotropy although the first-order magneto-structural transition is still seen at ≈ 540 K. Room temperature structural studies show that the Ru-Ru structural dimerization arrangement is also changed in the Na substituted samples. While the Li_2RuO_3 shows 2 short and 4 long Ru-Ru bonds on each honeycomb in an armchair pattern as previously seen^{20,22}, the Na doped samples show 4 short and 2 long Ru-Ru bonds on each honeycomb in an arrangement which can be viewed as two inter-penetrating armchair patterns.

II. EXPERIMENTAL DETAILS

The single crystalline samples of $(\text{Li}_{1-x}\text{Na}_x)_2\text{RuO}_3$ ($x = 0, 0.05$) have been synthesized. The starting materials were Li_2CO_3 (99.995% Alfa Aesar, Na_2CO_3 (99.995%

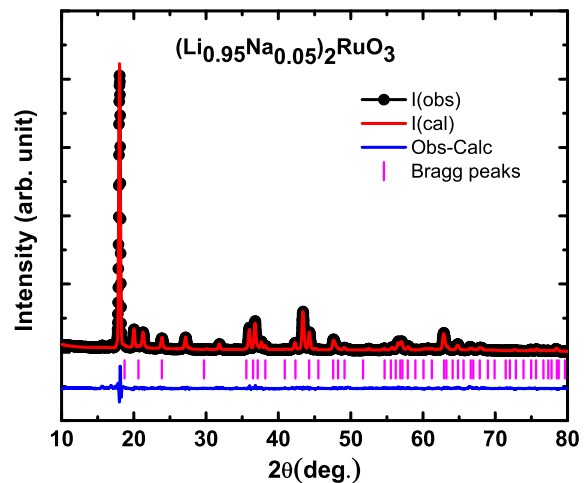


FIG. 1: (Color online) Rietveld refinements of powder x-ray diffraction data for $(\text{Li}_{0.95}\text{Na}_{0.05})_2\text{RuO}_3$. The solid circles represent the observed data, the solid lines through the data represent the fitted pattern, the vertical bars represent the peak positions, and the solid curve below the vertical bars is the difference between the observed and the fitted patterns.

Alfa Aesar) and Ru metal powder (99.95% Alfa Aesar). Single crystals were grown using a self flux growth method. Off-stoichiometric amounts of starting materials were mixed and placed in an alumina crucible with a lid, heated to 750 °C for 24 h for calcination and then furnace cooled to room temperature. Crystal growth was done by keeping the calcined mixture for long periods (70–80 h) at temperatures between 1000 °C – 1050 °C after which the furnace is turned off and allowed to cool to room temperature. Shiny plate like single crystals (size $\sim 0.5 \times 0.5 \times 0.03$) were found to grow on top of semi-melted polycrystalline powder. Growth of crystals with higher Na concentrations were tried but were not successful. The structure and composition of the resulting samples were checked by single-crystal and powder x-ray diffraction (PXRD), and chemical analysis using energy dispersive x-ray (EDX) analysis with a JEOL scanning electron microscope (SEM). The PXRD was obtained by a Rigaku diffractometer with Cu K_α radiation in 2θ range from 10° to 90° with 0.02° step size. Anisotropic magnetic susceptibility measurements upto $T = 1000$ K were measured on a collection of co-aligned crystals with total mass ≈ 12 mg using the VSM Oven option on a Quantum Design physical property measurement system.

III. RESULTS

A. Crystal Structure and Chemical Analysis

From room temperature single crystal and powder x-ray diffraction, we conclude that all samples adopt the $P2_1/m$ space group. A full single crystal refinement was not possible because the crystals have multiple twins ro-

TABLE I: Wyckoff position for $(\text{Li}_{0.95}\text{Na}_{0.05})_2\text{RuO}_3$ obtained from Rietveld refinements of polycrystal x-ray data at 300 K

Atom	Wyckoff	x	y	z	Occ	B (\AA)
Ru	4f	0.2467(7)	0.0776(8)	-0.0038(7)	1	0.0265
Li1	2e	0.7857(5)	0.25	-0.0295(8)	0.95	0.0800
Na1	2e	0.7857(5)	0.25	-0.0295(8)	0.05	0.0900
Li2	4f	0.0661(3)	0.25	0.6213(7)	1	0.0034
Li3	2e	0.6887(3)	0.0523(5)	0.4685(6)	1	0.0020
O1	4f	0.7812(6)	0.0644(7)	0.2831(8)	1	0.0043
O2	4f	0.7502(5)	0.0957(7)	0.7931(2)	1	0.0060
O3	2e	0.3124(7)	0.25	0.2688(5)	1	0.0088
O4	2e	0.2396(8)	0.25	0.2373(4)	1	0.0080

tated around the c^* axis. However, it was possible to determine the space group and cell parameters using single crystal diffraction. Cell parameters were also obtained by performing Rietveld refinements of the PXRD patterns obtained on the crushed crystals. Fig.1 shows representative results of Rietveld refinement of the PXRD patterns for $(\text{Li}_{0.95}\text{Na}_{0.05})_2\text{RuO}_3$. The fractional atomic positions obtained from the refinement are given in Table I. The unit cell parameters and the relevant bond lengths extracted from Rietveld refinement of the powder diffraction data are listed in Table II. The cell parameters change significantly (specially the a -axis) as Li is partially replaced by Na. The presence of Na in the doped crystals and its concentration relative to Ru was confirmed using energy dispersive X-ray spectroscopy on several spots on the same crystal and on several crystals and was found to be close to the nominal concentration targeted in the starting material.

The room temperature crystal structure of Li_2RuO_3 and Li viewed perpendicular to the honeycomb planes is shown in Fig. 2 to highlight the Ru-Ru dimerization pattern. For Li_2RuO_3 we find, consistent with previous work, that one (d_2) out of the three inequivalent Ru-Ru bonds is considerably shorter compared to the other two which are of similar lengths. Surprisingly, for just 5% Na substitution for Li, the dimerization pattern changes and we now have two short (d_2 and d_3) and one long bonds. The Ru-Ru bond lengths are given in Table II and the dimerization patterns shown in Figs. 2 (a) and (b), respectively. For Li_2RuO_3 as observed²⁰ and explained²² previously the dimers on the d_2 bond form an armchair pattern. For the Na substituted sample, both d_2 and d_3 bonds dimerize and form inter-penetrating armchairs which run along the a -axis.

TABLE II: Summary of Lattice Parameters and relevant bond lengths of $(\text{Li}_{1-x}\text{Na}_x)_2\text{RuO}_3$ ($x \approx 0, 0.05$)

Sample	Li_2RuO_3	$(\text{Li}_{0.95}\text{Na}_{0.05})_2\text{RuO}_3$
Space Group	$P2_1/m$	$P2_1/m$
a (\AA)	4.920(4)	4.934(5)
b (\AA)	8.781(7)	8.774(4)
c (\AA)	5.893(3)	5.895(6)
β (deg)	124.36(4)	124.42(6)
V (\AA^3)	210.452(5)	210.452(5)
$\text{Ru} - \text{Ru}$ (\AA)		
d_1	3.024	3.025
d_2	2.632	2.812
d_3	2.937	2.823

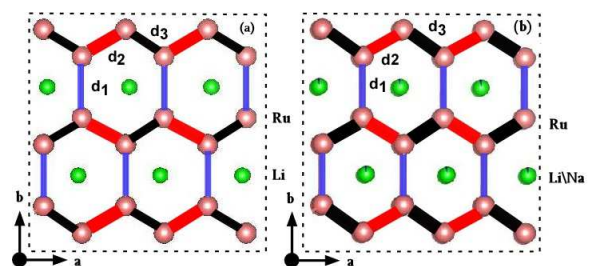


FIG. 2: (Color online) Room temperature structure of (a) Li_2RuO_3 and (b) $(\text{Li}_{0.95}\text{Na}_{0.05})_2\text{RuO}_3$ viewed perpendicular to the Ru honeycomb network in the ab -plane. There are three inequivalent Ru-Ru bonds in the honeycomb network labeled as d_1 (blue), d_2 (red), and d_3 (black). For Li_2RuO_3 , the Ru-Ru dimerization happens on the d_2 bonds (shown as the thicker red bonds in (a)) which are considerably shorter than d_1 and d_3 which are of similar length. The armchair pattern observed for Li_2RuO_3 is consistent with that observed earlier²⁰. For $(\text{Li}_{0.95}\text{Na}_{0.05})_2\text{RuO}_3$ the dimerization pattern changes and there are two short bonds d_2 (thick red) and d_3 (thick black) and one long bond d_1 (thin blue). The dimer arrangement can be viewed as two inter-penetrating armchair patterns.

B. Magnetic susceptibility

1. Li_2RuO_3

The magnetic susceptibility χ versus T data for Li_2RuO_3 measured in an applied magnetic field $H = 5$ T applied parallel to the honeycomb plane (χ_{\parallel}) or perpendicular to the honeycomb plane (χ_{\perp}) are shown in Fig. 3. Figure 3(a) shows the χ_{\perp} data from 300 K to 1000 K and the χ_{\parallel} data from 2 K to 1000 K. Both sets of data were measured while cooling down from 1000 K. The first thing to note is that $\chi_{\parallel} > \chi_{\perp}$ for all temperatures. The $\chi(T)$ behavior at high temperatures is not Curie-Weiss like as expected for a paramagnet. Instead the $\chi(T)$ behavior is consistent with a quasi-two-dimensional magnetic system having stronger in-plane interactions. We

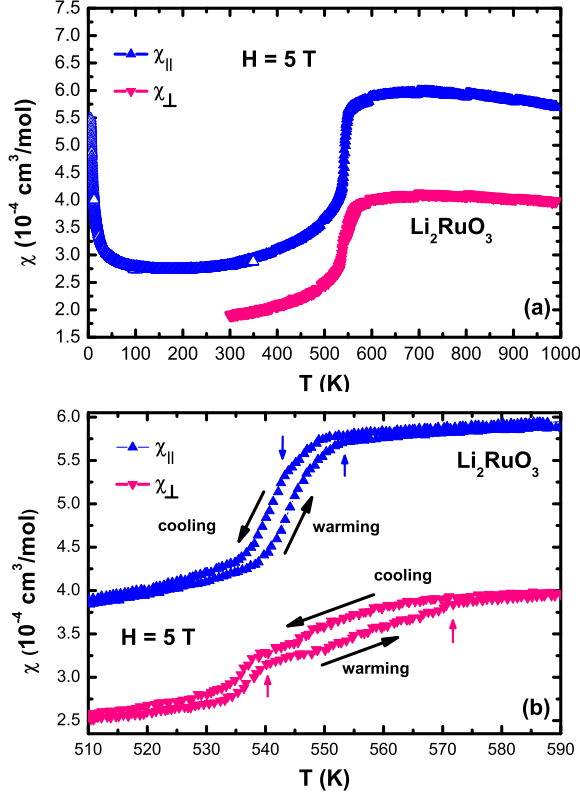


FIG. 3: (Color online) (a) Anisotropic Magnetic susceptibility $\chi_{||}$ and χ_{\perp} versus T measured at in a magnetic field of 5 T for Li_2RuO_3 between $T = 2$ K and 1000 K. (b) $\chi_{||}$ and χ_{\perp} versus T in the temperature range 510 K to 590 K to highlight the behaviour near the transition.

also see evidence for a transition involving an abrupt drop in χ below about 550 K. This is a signature of the magneto-structural transition observed previously for polycrystalline samples²⁰. The magneto-structural transition has been previously reported to involve a structural change below 540 K from $C2/m$ to $P2_1/m$ symmetry and a simultaneous Ru-Ru dimerizations with spin-singlet formation²⁰. The abrupt drop in χ at the transition is consistent with Ru-Ru spin-singlet formation. The magnitude of the drop can be quantified by χ_{\min}/χ_{\max} and is ≈ 0.45 for both $\chi_{||}$ and χ_{\perp} . Below 300 K, the $\chi(T)$ is T independent and small but finite. This T independent finite value ($\chi_{||} \approx 2.75 \times 10^{-4} \text{ cm}^3/\text{mol}$) is most likely a Van Vleck paramagnetic contribution⁷.

In Fig. 3 (b) we show the χ_{\perp} and $\chi_{||}$ data on an expanded scale around the region of the transition. Data were recorded while warming from 300 K to 1000 K and then while cooling back again at a rate of 5 K/min. We see that there is a thermal hysteresis between the warming and cooling data indicating the first order nature of the phase transition. The transition temperatures obtained by taking derivatives of the data (not shown) are listed in Table III. For $\chi_{||}$ we get the transition temperatures 544 K for warming and maybe a double transition

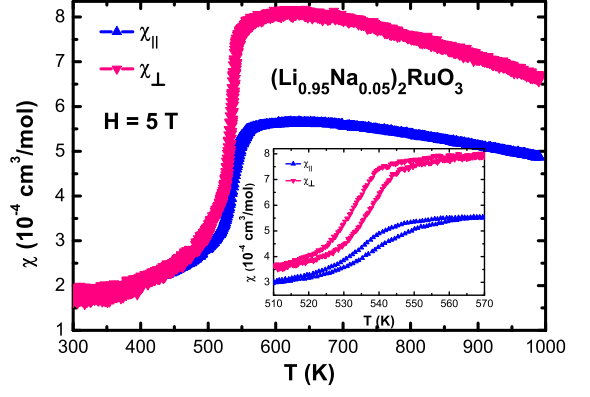


FIG. 4: (Color online) Anisotropic Magnetic susceptibility $\chi_{||}$ and χ_{\perp} versus T measured at in a magnetic field of 5 T for $(\text{Li}_{0.95}\text{Na}_{0.05})_2\text{RuO}_3$ between $T = 300$ K and 1000 K. The inset shows the $\chi_{||}$ and χ_{\perp} versus T in the temperature range 510 K to 570 K to highlight the behaviour near the transition.

TABLE III: Temperatures of the peaks in $d\chi/dT$ for $\chi_{||}$ and χ_{\perp} of single crystalline Li_2RuO_3 at $H = 5$ T

Magnetic susceptibilities	T_1	T_2
Li_2RuO_3		
$\chi_{ }$ (heating)	540 K	546 K
$\chi_{ }$ (cooling)		544 K
χ_{\perp} (heating)	538.3 K	561 K
χ_{\perp} (cooling)	537.8 K	555 K
$(\text{Li}_{0.95}\text{Na}_{0.05})_2\text{RuO}_3$		
$\chi_{ }$ (heating)	542 K	
$\chi_{ }$ (cooling)	535 K	
χ_{\perp} (heating)	538 K	
χ_{\perp} (cooling)	531 K	

at 540 K and 546 K for cooling measurements. The thermal hysteresis is about 5 K. For χ_{\perp} the situation is more complex. The transition clearly happens in two steps as indicated by the vertical arrows close to the data in Fig. 3(b) signalling the onset of the two transitions. A derivative of the χ_{\perp} data shows two peaks which are taken as the approximate transition temperatures and listed in Table III. We note that the lower transition is sharp and is not accompanied by any significant thermal hysteresis whereas the higher temperature transition is broad and clearly hysteretic. The hysteresis in the higher temperature transition is about 6 K as observed for the $\chi_{||}$ data. We will return to a discussion of these data in a later section.

2. $(\text{Li}_{0.95}\text{Na}_{0.05})_2\text{RuO}_3$

The magnetic susceptibility χ versus T data for $(\text{Li}_{0.95}\text{Na}_{0.05})_2\text{RuO}_3$ measured between 300 K to 1000 K

in an applied magnetic field $H = 5$ T applied parallel to the honeycomb plane ($\chi_{||}$) or perpendicular to the honeycomb plane (χ_{\perp}) are shown in the main panel in Fig. 4. Surprisingly, with only a 5% Na substitution for Li, the anisotropy is reversed ($\chi_{\perp} > \chi_{||}$) compared to what was observed for Li_2RuO_3 . The magneto-structural transition can be seen in both sets of data. The Fig. 4 inset shows the $\chi_{||}$ and χ_{\perp} data in the temperature range 510 K to 570 K to highlight the transition. Data were recorded while warming from 300 K to 1000 K and then while cooling back again at a rate of 5 K/min. We see that there is a thermal hysteresis between the warming and cooling data indicating that the first order nature of the phase transition persists in Na substituted samples. Peaks in the derivatives of the $\chi(T)$ data are taken as the approximate transition temperatures and are given in Table III.

IV. SUMMARY AND DISCUSSION

We have grown the first single crystals of $(\text{Li}_{1-x}\text{Na}_x)_2\text{RuO}_3$ ($x = 0, 0.05$) crystallizing in the $P2_1/m$ structure at room temperature and showing a magneto-structural transition at high temperatures. Using magnetic susceptibility χ measurements for temperatures $T \leq 1000$ K we observe that for Li_2RuO_3 , $\chi_{||} > \chi_{\perp}$. Additionally, we observe a first-order high temperature coupled magneto-structural transition which seems to occur in two steps. This is most evident in the χ_{\perp} data. The higher temperature transition has an onset as high as $T > 570$ K and a mid-point around $T \approx 561$ K as seen by the peak in $d\chi_{\perp}/dT$ measured while warming up to 1000 K. This high temperature transition is hysteretic with a thermal hysteresis of 6 K indicating its first-order nature. The lower temperature transition in χ_{\perp} occurs at $T \approx 538$ K, is very sharp, is accompanied by an abrupt fall in χ , and with almost

no thermal hysteresis. These observations suggest that the higher temperature, hysteretic transition is the structural dimerization transition while the lower temperature transition where we observe a sharp fall in χ is the magnetic transition involving Ru-Ru singlet formation. Thus for Li_2RuO_3 the two transitions most likely occur at slightly different temperatures with the structural dimerization transition occurring first and triggering the magnetic Ru-Ru singlet formation. The onset temperature of 570 K is much higher than previously observed (≈ 540 K) and indicates the high quality of the samples.

Just a 5% substitution of Na for Li leads to interesting magnetic and structural changes. The high temperature $\chi(T)$ data show that the magnetic anisotropy is reversed compared to Li_2RuO_3 with $\chi_{\perp} > \chi_{||}$ for $(\text{Li}_{0.95}\text{Na}_{0.05})_2\text{RuO}_3$. The arrangement of Ru-Ru dimers on the honeycomb lattice also changes. For Li_2RuO_3 Rietveld refinements of room temperature powder X-ray data reveal that one (d_2) out of the three inequivalent Ru-Ru bonds on the honeycomb lattice is shortened compared to the other two which are almost equal to each other as can be seen in Table II. For $(\text{Li}_{0.95}\text{Na}_{0.05})_2\text{RuO}_3$ we find that two (d_2 and d_3) out of the three Ru-Ru bonds are smaller and almost equal while the third is much larger. The armchair arrangement of the dimers in Li_2RuO_3 is consistent with previous reports²⁰⁷. The dimer arrangement in $(\text{Li}_{0.95}\text{Na}_{0.05})_2\text{RuO}_3$ can be viewed as two inter-penetrating armchairs formed on the d_2 and d_3 bonds, respectively. This suggests a possible change in the orbital ordering pattern for the Na substituted sample.

a. Acknowledgments.— We thank the X-ray facility at IISER Mohali for powder XRD measurements. YS acknowledges DST, India for support through Ramanujan Grant #SR/S2/RJN-76/2010 and through DST grant #SB/S2/CMP-001/2013. KM acknowledges UGC India for a fellowship.

-
- ¹ G. Jackeli, and G. Khaliullin, Phys. Rev. Lett. **102**, 017205 (2009).
 - ² A. Shitade, H. Katsura, J. Kunes, X.-L. Qi, S.-C. Zhang, and N. Nagaosa, Phys. Rev. Lett. **102**, 256403 (2009).
 - ³ D. A. Pesin and Leon Balents, Nature Phys. **6**, 376 (2010).
 - ⁴ X. Wan, A. M. Turner, A. Vishwanath, S. Y. Savrasov, Phys. Rev. B **83**, 205101 (2011).
 - ⁵ A. Kitaev, Ann. Phys. **321**, 2 (2006).
 - ⁶ J. Chaloupka, G. Jackeli, and G. Khaliullin, Phys. Rev. Lett. **105**, 027204 (2010).
 - ⁷ Y. Singh, and P. Gegenwart, Phys. Rev. B **82**, 064412 (2010).
 - ⁸ Y. Singh, S. Manni, J. Reuther, T. Berlijn, R. Thomale, W. Ku, S. Trebst, and P. Gegenwart, Phys. Rev. Lett. **108**, 127203 (2012).
 - ⁹ S. H. Chun, J.-W. Kim, J. Kim, H. Zheng, C. Stoumpos, C. Malliakas, J. F. Mitchell, Kavita Mehlaawat, Yogesh Singh, Y. Choi, T. Gog, A. Al-Zein, M. Moretti Sala, M. Krisch, J. Chaloupka, G. Jackeli, G. Khaliullin, and B. J. Kim, Nature Physics **11**, 3322 (2015).
 - ¹⁰ A. Banerjee, C. A. Bridges, J.-Q. Yan, A. A. Aczel, L. Li, M. B. Stone, G. E. Granroth, M. D. Lumsden, Y. Yiu, J. Knolle, S. Bhattacharjee, D. L. Kovrizhin, R. Moessner, D. A. Tennant, D. G. Mandrus, and S. E. Nagler, Nature Materials (2016) doi:10.1038/nmat4604.
 - ¹¹ S. Nath Gupta, P. V. Sriluckshmy, K. Mehlaawat, A. Balodhi, D. K. Mishra, D.V.S. Muthu, S. R. Hassan, Y. Singh, T. V. Ramakrishnan, and A. K. Sood, arXiv:1408.2239 (2014).
 - ¹² L. J. Sandilands, Y. Tian, K. W. Plumb, Young-June Kim, and K. S. Burch, Phys. Rev. Lett. **114**, 147201 (2015).
 - ¹³ Kavita Mehlaawat, G. Sharma, and Yogesh Singh, Phys. Rev. B **92**, 134412 (2015).
 - ¹⁴ Hechang Lei, Wei-Guo Yin, Zhicheng Zhong, and Hideo Hosono, Phys. Rev. B **89**, 020409(R) (2014).
 - ¹⁵ K. M. Mogare, K. Friesse, W. Klein, and M. Jansen, Z.

- Anorg. Allg. Chem. **630**, 547 (2004).
- ¹⁶ J. C. Wang, J. Terzic, T. F. Qi, F. Ye, S. J. Yuan, S. Aswartham, S. V. Streltsov, D. I. Khomskii, R. K. Kaul, and G. Cao, Phys. Rev. B **90**, 161110 (2014).
 - ¹⁷ J. F. Dulac, C. R. Acad. Sci. Paris, Ser. B **270**, 223 (1970).
 - ¹⁸ A. C. W. P. James and J. B. Goodenough: J. Solid State Chem. **74**, 287 (1988).
 - ¹⁹ I. Felner and I. M. Bradaric, Physica B **311**, 195 (2002).
 - ²⁰ Y. Miura, Y. Yasui, M. Sato, N. Igawa, and Kazuhisa Kakurai, J. Phys. Soc. Jpn. **76**, 033705 (2007).
 - ²¹ Y. Miura, M. Sato, Y. Yamakawa, T. Habaguchi, and Y. Ono, J. Phys. Soc. Jpn. **78**, 094706 (2009).
 - ²² G. Jackeli, and D. I. Khomskii, Phys. Rev. Rev. Lett. **100**, 147203 (2008).
 - ²³ S. A. J. Kimber, I. I. Mazin, Juan Shen, H. O. Jeschke, S. V. Streltsov, D. N. Argyriou, R. Valenti, and D. I. Khomskii, Phys. Rev. B, **89**, 081408(R) (2014).
 - ²⁴ J. Park, T-Y. Tan, D. T. Adroja, A. Daoud-Aladine, S. Choi, D-Y. Cho, S-H. Lee, J. Kim, H. Sim, T. Morioka, H. Nojiri, V. V. Krishnamurthy, P. Manuel, M. R. Lees, S.V. Streltsov, D.I. Khomskii, J-G. Park, arXiv:1604.04019 (2016).
 - ²⁵ Z. V. Pchelkina, A. L. Pitman, A. Moewes, E. Z. Kurmaev, Teck-Yee Tan, D. C. Peets, Je-Geun Park, and S. V. Streltsov, Phys. Rev. B **91**, 115138(2015).
 - ²⁶ M.-P. Jimenez-Segura, A. Ikeda, S. Yonezawa, and Y. Maeno, Phys. Rev. B **93**, 075133(2016).